Noise2Info: Noisy Image to Information of Noise for Self-Supervised Image Denoising

Jiachuan Wang [†], Shimin Di [†], Lei Chen [† *], Charles Wang Wai Ng [† *]
[†]The Hong Kong University of Science and Technology, Hong Kong SAR, China
[*]The Hong Kong University of Science and Technology (Guangzhou), Guangdong Province, China
jwangey@connect.ust.hk, sdiaa@connect.ust.hk, leichen@hkust-gz.edu.cn, charles.ng@ust.hk

Abstract

Unsupervised image denoising has been proposed to alleviate the widespread noise problem without requiring clean images. Existing works mainly follow the self-supervised way, which tries to reconstruct each pixel x of noisy images without the knowledge of x. More recently, some pioneer works further emphasize the importance of x and propose to weigh the information extracted from x and other pixels when recovering x. However, such a method is highly sensitive to the standard deviation σ_n of noise injected to clean images, where σ_n is inaccessible without knowing clean images. Thus, it is unrealistic to assume that σ_n is known for pursuing high model performance.

To alleviate this issue, we propose Noise2Info to extract the critical information, the standard deviation σ_n of injected noise, only based on the noisy images. Specifically, we first theoretically provide an upper bound on σ_n, while the bound requires clean images. Then, we propose a novel method to estimate the bound of σ_n by only using noisy images. Besides, we prove that the difference between our estimation with the true deviation goes smaller as the model training. Empirical studies show that Noise2Info is effective and robust on benchmark data sets and closely estimates the standard deviation of noise during model training.

1. Introduction

Generally, images are vulnerable to noise from latent observation and transmission [5, 26]. As an essential enhancement for digital images, image denoising aims to convert noisy images X to clean ones Y, where the image denoising model $\mathcal{F}(X)$ is expected to output the near clean image (i.e., $\mathcal{F}(X) \approx Y$). Assuming that clean images are available, deep learning models [23, 16] have been introduced to the image denoising task, and achieved outstanding performance over traditional methods [10, 11, 12] on the supervised image denoising task [31, 22, 14].

However, in real-world scenarios, only noisy images can be observed, i.e., we do not know whether an image has been contaminated or what the ground truth of a noisy image (a clean one) looks like. Thus, it is hard to apply the supervised deep learning approaches. To handle such cases, Noise2Noise [19] assumes that pairwise noisy images of one clean image can be accessible, which can be viewed as noisy supervision [29]. On the other hand, many papers assume that the distribution of noise is known, named noise model. A common setting for noise $n \sim \mathcal{N}$ is zero-mean ($\mu_n = 0$) with unknown standard deviation (σ_n) [17, 18, 29, 3]. The Gaussian and multiplicative Bernoulli noises have also been covered [21]. CBDNet [14] assumes that photographs have Poisson-Gaussian noise. However, their assumptions are not always held in reality and limit the applicability of their methods.

To enable models to denoise on a more practical scenario, recent works (e.g., *Noise2Self* [3], *Noise2Void* [17] and *Convolutional blind-spot network* [18]) develop self-supervised models mainly based on available noisy images. If a model $\mathcal{F}$ takes noisy image X as both input and target, it will quickly collapse to the identity function $\mathcal{F}(X) = X$. Instead, these papers use the idea of $\mathcal{J}-$*invariance* [3]. Loosely speaking, given noise image X, a $\mathcal{J}-$invariant model denoises each pixel $x \in X$ only based on any other pixels (i.e., using pixels from $X \backslash \{x\}$). This setting prevents model from learning the identity function. Though the pixels used for supervision are noisy, with many samples drawn from the same image distribution, the model is supposed to learn the expected ground truth value.

For the strictly $\mathcal{J}-$invariant model, each pixel is denoised without using the pixel itself, so that we call it external method. Based on the idea, many papers point out that the extracted information based on the pixel itself, which is the internal information of the pixel, can be utilized for better results [3, 18, 29]. *Noise2Same* [29] considers both the external and internal information to further outperform these purely external models. Formally, *Noise2Same* builds a self-supervised $\mathcal{L}(\mathcal{F}, X)$ (i.e., the loss of $\mathcal{F}$ w.r.t. X) on

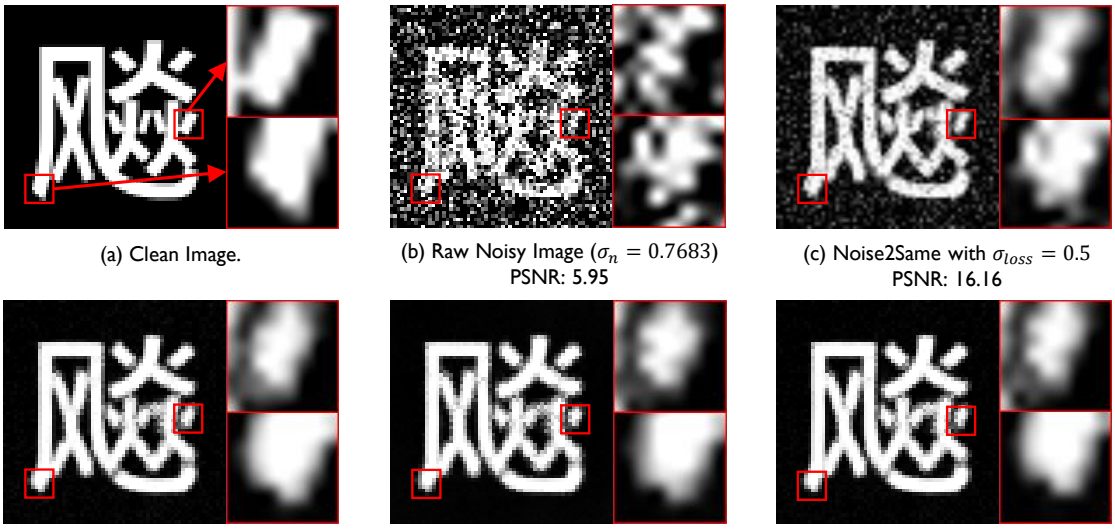

(a) Clean Image. (b) Raw Noisy Image ($\sigma_n = 0.7683$) PSNR: 5.95 (c) Noise2Same with $\sigma_{loss} = 0.5$ PSNR: 16.16

(d) Noise2Same with $\sigma_{loss} = \sigma_n$ PSNR: 19.00 (e) Noise2Same with $\sigma_{loss} = 1$ PSNR: 18.07 (f) Our Noise2Info with $\sigma_{loss} = 0.7783$ PSNR: 18.81

Figure 1: Motivation examples taken from Hànzì dataset to compare our output with Noise2Same under different σ_{loss}.

the top of internal loss $\mathcal{L}_{in}$ and external loss $\mathcal{L}_{ex}$ as:

$$\mathcal{L}(\mathcal{F}, X) = \mathcal{L}_{in} + 2\sigma_{loss}\mathcal{L}_{ex}, \tag{1}$$

which is an upper bound of the typical supervised loss. For a normalized noisy image, σ_{loss} is proved to be the standard deviation of its noise σ_n. As σ_n is not available, *Noise2Same* uses $\sigma_{loss} = 1$ by default instead. Note that the closer σ_{loss} and σ_n are, the better the image denoising performance. As shown in Fig. 1, we show an image (Fig. 1 (a)) from Hànzì dataset and its noisy version (Fig. 1 (b)) with std of noise $\sigma_n = 0.7683$. When σ_{loss} is set to 0.5 and 1 (Fig. 1(c) and Fig. 1 (e)), the performances of *Noise2Same* are not so desirable compared with that of $\sigma_{loss} = \sigma_n$ (Fig. 1 (d)). However, σ_n can only be known when clean images are available, which contradicts the purpose of practical image denoising. Thus, it is hard to manually set σ_{loss} closed to σ_n for better performance, especially when there is no clean image for tuning σ_{loss}. Besides, as shown in Fig. 4 of [29], the quality of denoised images is highly sensitive to σ_{loss}.

In this paper, we aim to solve the above issue to enable the image denoising model to work well when no clean image nor noise model is available. Motivated by the observation on σ_n, we propose *Noise2Info* to derive σ_n-related information by only taking the noisy images as inputs, which has not been studied in existing works. First, we theoretically estimate the upper bound of σ_n in *Noise2Info*. Then, based on the estimation, *Noise2Info* can dynamically update σ_{loss} during the model training. In addition, we prove that the gap between estimated upper bound with the true standard deviation will become smaller as model training, leading to a convergent stable result. The empirical study shows that *Noise2Info* outperforms other self-supervised methods and achieves comparable results over the supervised methods. Especially, *Noise2Info* even beats all self-supervised methods including *Noise2Same* with known σ_n on the two benchmark data sets where noises are signal-dependent and not zero-mean, which validates the generality of our method. We also synthesize data sets with various noise types and scales. As shown in Tab. 4 and Tab. 9, the gap between σ_n and σ_{loss} estimated by Noise2info is pretty small (< 0.02), which verifies that Noise2info can indeed estimate σ_n only based on noisy images.

Notations. In this paper, we denote the lower case a to the scalar and the upper case $A \in \mathbb{R}^m$ to the vector. We use the superscript $A^{(i)} \in \mathbb{R}^m$ to denote the i-th sample, the bold font $\mathbf{A}$ to the set, like $\mathbf{a} = \{a^{(1)}, \ldots, a^{(q)}\}$ and $\mathbf{A} = \{A^{(1)}, \ldots, A^{(q)}\}$. The subscript $A_j^{(i)}$ is j-th element of $A^{(i)}$. The Fraktur case $\mathcal{A}$ denotes the function. Besides, $\tilde{A}$ denotes the output of the denoising model, and the star A^* denotes the estimation.

2. Background and Related Works

2.1. Image denoising

We categorize various image denoising models based on the form of supervision below.

Unsupervised Denoising. Many traditional methods based on the assumptions of smoothness and self-similarity of the image fall into this category. These models do not

need to be trained and thus have a wide range of applicabilities but their performance is unstable [5, 26]. Various filters can be viewed as denoisers, such as Mean filter, Median filter, and Gauss filter [13]. The non-local means algorithm [4] is proposed as a more powerful mean filter. It outputs the mean of weighted pixels from the whole image instead of neighbors, where the weights are set according to similarity. BM3D algorithm [10] further improves the results. Similar image fragments are grouped and stacked as blocks. These blocks are further transferred to frequency space and applied with thresholding to filter high frequency noise. BM3D has many hyperparameters including the standard deviation of noise for thresholding, which limits its applicability for blind denoising.

Denoising with Paired Input and Target. The image denoising can be viewed as a general regression task with paired noisy and clean images (X, Y), where $X, Y \in \mathbb{R}^m$ and $m = h \times w \times c$ is the number of pixels of each RGB image. The noisy image can be viewed as a combination of the clean image and a noise map N ($X = Y + N$), where $N \in \mathbb{R}^m$ and the pixels of N are *i.i.d.*. The denoising model $\mathcal{F} : \mathbb{R}^m \to \mathbb{R}^m$ aims to minimize the loss function:

$$\mathcal{L} = \mathbb{E}_{X,Y}||\mathcal{F}(X) - Y||, \tag{2}$$

where $||\cdot||$ is the distance metric. *DnCNN* [31] learns the residual noise map $\tilde{N} \in \mathbb{R}^m$ and uses $X - \tilde{N}$ as the final output. *CBDNet* [14] assumes that the noise map $\tilde{N}$ is more likely to follow the mixed Poisson-Gaussian distribution.

However, clean images are usually not available in real-world scenarios. *Noise2Noise* [19] builds the denoising model with noisy pairs (X_1, X_2), which has loss function:

$$\mathcal{L} = \mathbb{E}_{X_1,X_2}||\mathcal{F}(X_1) - X_2||. \tag{3}$$

As long as the pair of noisy samples have zero-mean and independent noise, *Noise2Noise* proves that training on paired noisy images is the same as training on noisy and clean images because of the proof $\mathbb{E}[X_2|X_1] = Y$. Under such noisy supervision, *Noise2Noise* even outperforms the supervised models trained on clean images of some datasets.

Self-supervised Denoising. It is still hard to hold the assumption of *Noise2Noise* that two or more samples with independent noise for a clean image exist. *Noise2Self* [3] first proposes the $\mathcal{J}$-invariance to handle a more general and realistic case, which trains denoising models only with one noisy observation, i.e., self-supervised image denoising.

Definition 1 ($\mathcal{J}$-invariance)**.** *Given a noisy image $X \in \mathbb{R}^m$, let $\mathcal{J} = \{J^{(1)}, J^{(2)}, \cdots, J^{(k)}\}$ be the non-intersecting partition of image X, and X_J be the pixels in the partition $J \in \mathcal{J}$, i.e., $concatenate(X_{J^{(1)}}, \ldots, X_{J^{(k)}}) = X$. Then, let $J^c = \mathcal{J}\backslash\{J\}$ denote the complement of J. The $\mathcal{J}$-invariant function is defined as:*

$$[\mathcal{F}(X_{J^c})]_J = [\mathcal{F}(X)]_J, \forall J \in \mathcal{J}.$$

The $\mathcal{J}$-invariant function tries to recover pixels in partition J by only using information from other partitions X_{J^c}, which can be regarded as self-supervision. It can force the model to extract the correlation between the pixels of one partition with those of other partitions.

Based on the $\mathcal{J}$-invariance, the $\mathcal{J}$-invariant models *Noise2Self* [3], *Noise2Void* [17], and *ConvBS* [18] propose to minimize losses of the form:

$$\mathcal{L} = \mathbb{E}_X[\mathcal{L}(\mathcal{F}, X)], \tag{4}$$

where the model $\mathcal{F}$ is updated based only on each noisy image X. Generally, the pixels in clean images are highly correlated. Assuming that the noises in every pixel are independent, such $\mathcal{J}$-invariant models can eliminate the noise of a given pixel by leveraging the neighbor information of this pixel. To exclude the information of pixel itself, *Noise2Self* and *Noise2Void* use masks while *ConvBS* designs a special convolution layer with restricted receptive field.

2.2. Information exploration and Bound of Noise2Same

$\mathcal{J}$-invariant models only make use of external information, i.e., only X_{J^c} without X_J. Many papers point out that these models clearly waste the internal information, i.e., the information of the pixel itself X_J, which can further improve the result [3, 18, 29]. *Noise2Self* [3] states that a linear combination of X_J and $\mathcal{F}(X_{J^c})$ improves the result when the standard deviation of noise σ_n is known. *ConvBS* [18] can improve the result with post-processing if the noise model is known. The advanced Noise2Same [29] proposes a theoretical bound over the loss in Eq. (2), which combines external and internal information:

$$\begin{aligned}
&\mathbb{E}_{X,Y}\left[||\mathcal{F}(X) - Y||^2 + ||X - Y||^2\right] \\
\leq &\mathbb{E}_X||\mathcal{F}(X) - X||^2 \\
&+ 2\sigma_n \cdot m\mathbb{E}_J\left[\mathbb{E}||\mathcal{F}(X)_J - \mathcal{F}(X_{J^c})_J||^2/|J|\right]^{1/2} \\
= &\mathcal{L}_{in} + 2\sigma_n \cdot \mathcal{L}_{ex}.
\end{aligned} \tag{5}$$

We denote components on the left and right of Eq. (5) as $\mathcal{L}_{in}$ and $\mathcal{L}_{ex}$. $\mathcal{L}_{in}$ pushes the output $\mathcal{F}(X)$ similar to the noisy input X itself. $\mathcal{L}_{ex}$ leads to the output that depends more on X_{J^c} by restricting $\mathcal{F}(X)_J - \mathcal{F}(X_{J^c})_J$. However, without the information of standard deviation of noise σ_n, *Noise2Same* can only use $\sigma_{loss} = 1$ instead of σ_n. In this paper, we aim to estimate σ_n based on the noisy images.

3. Noise2Info

In this section, we first introduce a tractable estimation on the upper bound of σ_n. We analyze the tightness of the bound and demonstrate that the bound could be tighter during model training. Then, we utilize the estimated bound as σ_{loss} in Eq. 1, and introduce how we train the model.

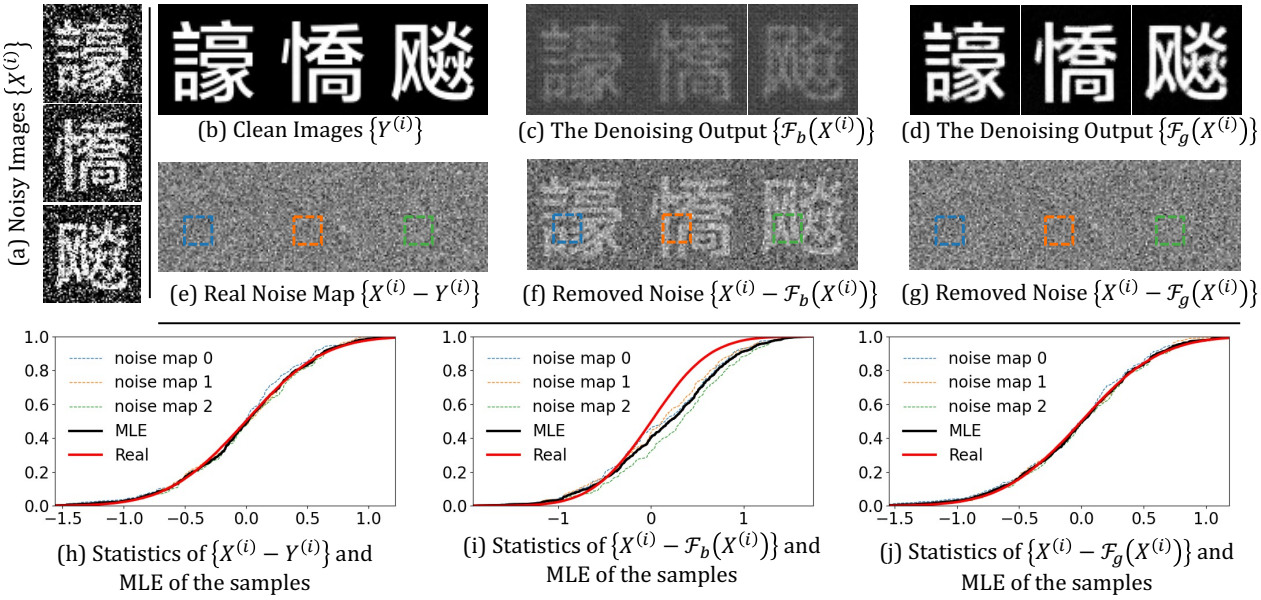

Figure 2: Examples taken from Hànzì. $\mathcal{F}_b(\cdot)$ is the denoising model *Noise2Info* trained within 10 batches, while $\mathcal{F}_g(\cdot)$ is trained until convergence. We plot the CDF of three noise maps (e.g., $\{X^{(i)} - Y^{(i)}\}$), their MLEs, and the real noise of the whole data set.

3.1. Upper Bound of σ_n

Recall that the performance of advanced image denoising model *Noise2Same* is affected by the manual setting of σ_{loss} as discussed in Sec. 1. The closer σ_{loss} and σ_n (i.e. the true standard deviation of the noise) is, the better the denoising performance. Thus, it is crucial to further investigate σ_n. First, we show the theoretical upper bound of σ_n in Lemma 1, where the proof is given in Appx. A.

Lemma 1 (Upper Bound of σ_n)**.** *Given a model $\mathcal{F}$ and a set of q normalized noisy images $\mathbf{X} = \{X^{(i)}\}_{i=1}^{p}$ with noise $n \sim \mathcal{N}$ i.i.d among all the dimensions, the standard deviation of noise σ_n can be upper bounded to:*

$$\sigma_n \leq (\mathcal{L}_{ex} + \sqrt{\mathcal{L}_{ex}^2 + m(\mathcal{L}_{in} - \mathbb{E}_{X,Y}[||\mathcal{F}(X) - Y||^2])})/m, \tag{6}$$

where m is the dimension of each image and $\mathcal{L}_{ex}$ and $\mathcal{L}_{in}$ are functions of X and $\mathcal{F}$ introduced in Sec. 2. Y is the clean image for each noisy image X.

In above lemma, $\mathcal{L}_{ex}$ and $\mathcal{L}_{in}$ are tractable with only noisy image X (see Eq. 5). However, term $\mathbb{E}_{X,Y}\left[||\mathcal{F}(X) - Y||^2\right]$ (i.e., $\mathcal{L}$ in Eq. 2) requires clean image Y, which is usually inaccessible as discussed in Sec. 2.1. To achieve an upper bound of σ_n, we need to estimate the lower bound of classic loss $\mathcal{L} = \mathbb{E}_{X,Y}\left[||\mathcal{F}(X) - Y||^2\right]$. We first rewrite $\mathcal{L}$ as:

$$\mathbb{E}_{X,Y}\left[||(X-Y)-(X-\mathcal{F}(X))||^2\right] = \mathbb{E}_{X,N}[||N-\tilde{N}(X)||^2], \tag{7}$$

where $N = X - Y$ is the true injected noise and $\tilde{N}(X) = X - \mathcal{F}(X)$ is the noise removed by the denoising model $\mathcal{F}$. Note that $\tilde{N}(X)$ can be observed for any given $\mathcal{F}$, while N is unknown due to the inaccessible clean image Y. We next introduce the motivational ideas of how to estimate Eq. 7.

As mentioned before, existing works assume that the noises contained in images are i.i.d. for any given dataset [17, 18, 29, 3]. Here we demonstrate several examples from the Hànzì [3] dataset in Fig. 2. Given 3 noisy images $\{X^{(i)}\}_{i=1}^{3}$ in Fig. 2 (a) and their corresponding clean images $\{Y^{(i)}\}_{i=1}^{3}$ in Fig. 2 (b), the true noise maps ($\{N^{(i)}\}_{i=1}^{3} = \{X^{(i)} - Y^{(i)}\}_{i=1}^{3}$) are shown in Fig. 2 (e). Then, we plot the cumulative distribution function (CDF) of each noise map N and the maximum likelihood estimation (MLE) of them in Fig. 2 (h). It is clear that they have similar patterns, i.e., follow the same real distribution (red line). Motivated by the assumption and empirical observation, we propose the idea that $X - \mathcal{F}(X)$ is expected to follow one same distribution if the image denoising model $\mathcal{F}$ is good. That is because $\mathcal{F}(X)$ tries to nearly output the clean image Y. If $X - Y$ follows a distribution, $X - \mathcal{F}(X)$ should also follow the same one as long as $\mathcal{F}(X) \approx Y$. In Eq. (7), noise maps $\{N^{(i)}\}_{i=1}^{q}$ are sampled from the same noise model. If the removed noises $\{\tilde{N}(X^{(i)})\}_{i=1}^{q}$s from

different images are of diverse distributions, no matter what distribution $\{N^{(i)}\}_{i=1}^{q}$ is drawn from, there would be a gap between N with $\tilde{N}(X)$, i.e., $\mathbb{E}_{X,Y}[||N-\tilde{N}(X)||^2]$ is large. Considering the lower bound of Eq. (7), the ideal case is that the distribution of N is exactly the MLE of samples in $\tilde{N}(X)$, i.e., $\mathbb{E}_{X,Y}[||N-\tilde{N}(X)||^2]=0$. Here we adopt it as our estimation.

Formally, given q noisy images $\mathbf{X}=\{X^{(i)}\}_{i=1}^{p}$, the denoising model $\mathcal{F}$ outputs q removed noise maps $\tilde{\mathbf{N}}=\{\tilde{N}(X^{(i)})\}_{i=1}^{q}$, where $\tilde{N}(X^{(i)})=X^{(i)}-\mathcal{F}(X^{(i)})\in\mathbb{R}^m$. Let $\tilde{\mathbf{n}}=\{\tilde{N}(X^{(i)})_j\}_{i,j=1}^{q,m}$ denote all removed noise pixels, where $\tilde{N}(X^{(i)})_j$ is the value of the j^{th} pixel in $\tilde{N}(X^{(i)})$. We derive the MLE of samples in $\tilde{\mathbf{n}}$, shown in the lemma below, where the proof is given in Appx. B.

Lemma 2 (MLE of samples from $\tilde{\mathbf{n}}$)**.** *We denote the maximum likelihood estimation of $\tilde{\mathbf{n}}$ as $n^*\sim\mathcal{N}^*$, which has distribution:*

$$P(n^*=\tilde{N}_j^{(i)})=(mq)^{-1}\qquad\forall\tilde{N}_j^{(i)}\in\tilde{\mathbf{n}},\tag{8}$$

where $\tilde{N}_j^{(i)}$ represents $\tilde{N}(X^{(i)})_j$ for short.

In statistics, to parameterize a given form of distribution, the output of the MLE makes the given samples most probable [24]. For Eq. (7), by replacing the real noise map N from unknown distribution $\mathcal{N}$ with MLE $\mathcal{N}^*$ based on $\tilde{N}(X)$, we get a smaller but tractable estimation of $\mathbb{E}_{X,N}[||N-\tilde{N}(X)||^2]$:

$$\mathbb{E}_{X,N^*}\left[||N^*-\tilde{N}(X)||^2\right]=\mathbb{E}_{N^*}[\mathbb{E}_X[\sum_{j=1}^{m}(N_j^*-\tilde{N}(X)_j)^2]].\tag{9}$$

The MLE enables us to estimate the expectation using Monte Carlo integration. Note that each sampled noise map N^* has m pixels, which could have arbitrary indices. We mathematically prove that the lower bound of Eq. (9) is the noise map N^* sorted in ascending order. The lemma is shown as follows and the proof is in Appx. C.

Lemma 3. *Given the sampled noise map N^* from $\mathcal{N}^*$, we sort the m pixels of the removed noise map $\tilde{N}(X)$ ($\{\tilde{N}(X)_j\}_{j=1}^{m}$) in increasing order and define the index list as $\{u_1,u_2,\cdots,u_m\}$, i.e., $\tilde{N}(X)_{u_1}\le\tilde{N}(X)_{u_2}\le\tilde{N}(X)_{u_3}\le\cdots\le\tilde{N}(X)_{u_m}$. Similarly, we define the index list for increasingly sorted sampled noise pixels $\{N_j^*\}_{j=1}^{m}$ as $\{v_1,v_2,\cdots,v_m\}$. We have:*

$$\begin{aligned}&\mathbb{E}_{N^*}[\mathbb{E}_X[\sum_{j=1}^{m}(N_j^*-\tilde{N}(X)_j)^2]]\\ \ge&\mathbb{E}_{N^*}[\mathbb{E}_X[\sum_{j=1}^{m}(N_{v_j}^*-\tilde{N}(X)_{u_j})^2]].\end{aligned}\tag{10}$$

Algorithm 1 Estimate the Upper Bound of σ_n as σ_{loss}

Input: The denoising model $\mathcal{F}(\cdot)$, k_u noisy images $\mathbf{X}=\{X^{(i)}\}_{i=1}^{p}$, the number of samples for MC integration k_{mc}
Initialize $\mathcal{L}_{in}\leftarrow 0$, $\mathcal{L}_{ex}\leftarrow 0$, $\tilde{\mathbf{n}}\in\{0\}^{k_u\times m}$, $E_l\leftarrow 0$ for the lower bound of $\mathbb{E}_{X,Y}\left[||\mathcal{F}(X)-Y||^2\right]$
for $i\leftarrow 1$ **to** k_u **do**
  Compute $\mathcal{L}_{in}$ and $\mathcal{L}_{ex}$ based on Eq. (5)
  $\tilde{\mathbf{n}}_{i,:}\leftarrow$ sorted $(\mathcal{F}(X_i)-X_i)$
end for
for $i\leftarrow 1$ **to** k_{mc} **do**
  $N^*\leftarrow$ Uniformly sample m values from $\tilde{\mathbf{n}}$ and sort them
  $E_l\leftarrow E_l+\sum_i||\tilde{\mathbf{n}}_{i:i+m}-N^*||^2$
end for
$E_l\leftarrow E_l/k_{mc}$ as the expectation
Feed $E_l,\mathcal{L}_{in},\mathcal{L}_{ex}$ to inequation (6) and get σ_{loss}
Return: The estimated of σ_n as σ_{loss}

Note that Eq. (10) can be unbiasedly estimated by Monte-Carlo (MC) integration with samples from $\mathcal{N}^*$.

In summary, Eq. (10) provides an estimation of lower bound on $\mathbb{E}_{X,Y}\left[||\mathcal{F}(X)-Y||^2\right]$ with Eq. (9) as the stepping stone. Then, we finally get a tractable estimation on the upper bound of σ_n after applying the lower bound on $\mathbb{E}_{X,Y}\left[||\mathcal{F}(X)-Y||^2\right]$ into Eq. (6).

3.2. Noise2Info Training

3.2.1 The Procedure of Estimating σ_n

The upper bound of σ_n has been introduced in Sec. 3.1. In Algo. 1, we show the steps of estimating σ_n for a fixed model $\mathcal{F}$. Note that the estimation is utilized as σ_{loss} in $\mathcal{L}(\mathcal{F},X)=\mathcal{L}_{in}+2\sigma_{loss}\mathcal{L}_{ex}$ (Eq. (1)). Thus, Noise2Info can avoid manually fixing a value to σ_{loss} as Noise2Same does. Instead, Noise2Info uses an estimate close to σ_n, which may further improve the denoising performance.

For each noisy image X, we derive its removed noise map $\tilde{N}(X)=\mathcal{F}(X)-X$, of which pixels are further sorted and collected to array $\tilde{\mathbf{n}}$. In each round of Monte Carlo integration, uniform sampling of $\tilde{\mathbf{n}}$ is exactly a sample of the maximum likelihood estimation derived in lemma 2. When we sort the sample and calculate its l_2 norm with regard to $\tilde{\mathbf{n}}$, we get a sample for the Eq. (10), which is accumulated in E_l. E_l is divided by k_{mc} as an expectation estimation of $\mathbb{E}_{X,Y}[||\mathcal{F}(X)-Y||^2]$. The terms on the right hand side of Eq. (6) are estimated, which outputs an upper bound of σ_n.

3.2.2 Training Framework

Sec. 3.2.1 introduces how to estimate σ_n for a fixed model $\mathcal{F}$. During training, the deep learning method updates the

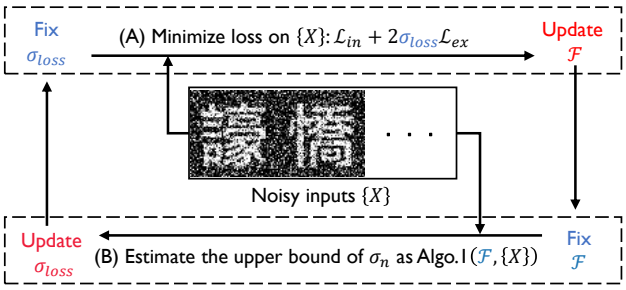

Figure 3: Training framework of Noise2Info: (A) update the denoising model $\mathcal{F}$ and (B) update the estimation σ_{loss}.

Algorithm 2 Noise2Info

Input: The denoising model $\mathcal{F}$, noisy images $\mathbf{X} = \{X^{(i)}\}_{i=1}^{p}$, the number of epochs k_r, the number of samples for model updation k_t and σ_n estimation k_u.
Initialize $\sigma_{loss} \leftarrow 1$.
for $i \leftarrow 1$ **to** k_r **do**
  Update $\mathcal{F}$ via loss $\mathcal{L}_{in} + 2\sigma_{loss}\mathcal{L}_{ex}$ with k_t samples.
  $\sigma^*_{loss} \leftarrow$ Algorithm 1($\mathcal{F}$, k_u noisy images, k_{mc})
  if $\sigma^*_{loss} < \sigma_{loss}$ **then**
    $\sigma_{loss} \leftarrow \sigma^*_{loss}$
  end if
end for
Return: model $\mathcal{F}$ for denoising

model every batch, where we may obtain many $\mathcal{F}$s. Among all estimations on the upper bound of σ_n, we prefer to choose models that can implicitly estimate tighter bounds (i.e., $\sigma_{loss} - \sigma_n$ is small). In the following proposition, we state the relationship between $\mathcal{F}$ and its estimation σ_{loss}, where proof is provided in Appx. D.

Proposition 1. *Assume that training model $\mathcal{F}$ under loss (5) pushes output $\mathcal{F}(X)$ closer to clean image Y. A more well-trained $\mathcal{F}$ will estimates a smaller σ_{loss} (i.e., tighter upper bound of σ_n).*

Based on above proposition, we can estimate tighter σ_{loss} when using a well-trained $\mathcal{F}$. Correspondingly, as discussed in Sec. 1, we can train more powerful $\mathcal{F}$ while feeding tighter estimation to Eq. (1). Recall the motivational observation in Fig. 2. Fig. 2 (i) demonstrates that the MLE of noise maps removed by $\mathcal{F}_b(\cdot)$ (only trained with 10 batches) cannot well fit the real one, but that of noise maps removed by well-trained $\mathcal{F}_g(\cdot)$ can fit as shown in Fig. 2 (j). This verifies that the gap between N with $\tilde{a}$ is small as long as the denoising model can nearly output the clean images.

Therefore, we propose to alternatively train the model $\mathcal{F}$ and estimate σ_n. We summarize the whole training framework of *Noise2Info* in Algo. 2 and Fig. 3. In each round, $\mathcal{F}$ is first updated with an upper bound of loss function (5), where σ_{loss} is applied instead of the unknown σ_n (Fig. 3(A)). Then, the model $\mathcal{F}$ is fixed and the gradient descent is turned off. k_u samples of noisy images are used for σ_{loss} updation according to Algo. 1(Fig. 3(B)). As each estimation is an upper bound of σ_n, we update the σ_{loss} once a smaller estimation is found.

Table 1: Data Statistics

Dataset	Channel	Pixel Range	#Tra/Tst Images
ImageNet	RGB	[0, 255]	60,000 / 978
Hànzì	Grey	[0,1]	54,385 / 7,770
BSD68	Grey	[0, 255]	3,168 / 68

4. Experimental Study

4.1. Experimental Setups

Dataset. We adopt the benchmark datasets including ImageNet ILSVRC 2012 Val [25], Hànzì [3], and BSD68[20], which are widely adopted in previous works [29, 3, 17, 8]. Besides that, we also conduct experiments on real world datasets SIDD [2], PolyU [30], and discuss another dataset Planaria in Appx. E. ImageNet are colored natural images injected with noise including Poisson noise ($\lambda = 30$), additive Gaussian noise ($\mu = 0, \sigma = 60$), and Bernoulli noise ($p = 0.2$). Hànzì dataset is generated by adding noise to grey images of Chinese characters, where the main experiment applies Gaussian noise ($\mu = 0, \sigma = 0.7$) and Bernoulli noise ($p = 0.25$). The output images are further clipped into $[0, 1]$ (set values to 1 if they are larger than 1 and to 0 if they are smaller than 0). BSD68 dataset contains grey natural images with only Gaussian noise ($\sigma = 25$). We summarize the statistic of these datasets in Tab. 1.

Baselines and Implementations. We compare *Noise2info* with traditional methods *NLM* [4] and *BM3D* [10], supervised methods *Noise2True* defined in *Noise2Noise* [19], self-supervised methods *Noise2Void* [17], *Noise2Self* [3], *ConvBS* [18], and *Noise2Same* [29]. We follow the *Noise2Same*, *Noise2Void*, and *Noise2Self* to use Uniform Pixel Selection as the masking strategy. The real values of masked pixels are invisible to the model, which forces the model to use external information to denoise it ($\mathcal{J}$-invariant). *Noise2Same* replaces the masked pixels with *i)* local average excluding the center pixel (donut) for BSD68; and *ii)* Gaussian random value for ImageNet and Hànzì, which get the best performance. We show the results under both donut and random replacements, named *Noise2Info*-D and *Noise2Info*-R. One can refer to [29] for the detailed setting of other methods.

All the codes are implemented in Tensorflow [1], which are available in the supplementary materials. The train-

Table 2: The comparison of image denoising on three data sets. The best scores are in **bold** font and the second-best scores are underlined in self-supervised models. *ConvBS* [18] does not contain the step that requires the noise model. As σ_{loss} for *Noise2Same* can only be set to 1 with unknown σ_n, we take *Noise2Same*($\sigma_{loss} = \sigma_n$) as a special category.

Category	Model	Data set		
		ImageNet	Hànzì	BSD68
Traditional method	Noisy Images without Denoising	9.70	6.45	20.19
	NLM [4]	18.04	8.41	22.73
	BM3D [10]	18.74	10.90	28.59
Clean-supervision	Noise2True	23.43	16.00	29.11
Noisy-supervision	Noise2Noise [19]	23.39	14.30	28.86
Self-supervision + noise information	Noise2Same-R ($\sigma_{loss} = \sigma_n$) [29]	22.57	14.14	27.77
	Noise2Same-D ($\sigma_{loss} = \sigma_n$) [29]	22.58	14.08	28.03
Self-supervision	ConvBS [18]	20.89	10.70	27.15
	Noise2Void [17]	21.63	13.84	27.28
	Noise2Self-R [3]	21.42	13.98	25.21
	Noise2Self-D [3]	21.48	14.11	**28.33**
	Noise2Same-R ($\sigma_{loss} = 1$) [29]	22.49	14.38	27.10
	Noise2Same-D ($\sigma_{loss} = 1$) [29]	22.57	14.36	27.24
	Noise2Info-R	22.51	**14.43**	27.57
	Noise2Info-D	**22.60**	**14.43**	27.74

Table 3: The information of groundtruth σ_n and σ_{loss} derived by *Noise2Info* on three data sets.

Dataset	*Noise2Info*-R	*Noise2Info*-D	Training Set		Test Set	
	σ_{loss}	σ_{loss}	μ_n	σ_n	μ_n	σ_n
ImageNet	0.9004	0.9015	-1.3726	0.9832	-0.0560	0.9483
Hànzì	0.9596	0.9592	-0.1815	1.2193	-0.1820	1.2193
BSD68	0.5357	0.5309	0	0.5043	-0.0020	0.4678

ing is conducted on one machine with 4 NVIDIA V100 GPUs. We follow the setting of *Noise2Same* [29] to employ *GVTNets* [27] as the denoising neural network. We set $k_t = 900$ and $k_u = 100$, and the total number of training steps ($(k_t + k_u) * k_r$) to be the same as *Noise2Same*.

Evaluation Results. Peak Signal-to-Noise Ratio (PSNR) is used as the evaluation metrics following previous works [29, 19, 17, 3]. For denoising, PSNR is the log-transformation of the ratio between the square of maximum value of a clean image and its mean-squared error against the noisy image: $PSNR(\mathcal{F}(X), Y) = 10 \cdot \log_{10}(|\max(Y)|^2/||\mathcal{F}(X) - Y||^2)$, where the larger PSNR value indicates the smaller $||\mathcal{F}(X) - Y||^2$, i.e., better image denoising performance.

4.2. Main Empirical Study

We show the main results in Tab. 2 and demonstrate some visual cases in Appx. F.1. Among the traditional methods, *NLM* has weak performance compared with learning-based methods. As discussed in Sec. 2.1, *BM3D* relies on the additional information σ_n for denoising, which leads to better performance and even beats all the self-supervised methods on BSD68. Notably, the mean of noises in BSD68 is zero, which is suitable for *BM3D*. But learning-based methods still outperform *BM3D* on the other two datasets. Overall, *Noise2True* outperforms all the other methods while *Noise2Noise* outperforms most of the self-supervised methods. However, it is not realistic to assume that either clean images or two noisy images sampled from one clean image are available in the real world.

Among the self-supervised methods, *Noise2Info* and *Noise2Same* outperform the other on ImageNet and Hànzì. On BSD68, only *Noise2Self* with Donut beat them. However, *Noise2Self*-Donut falls behind our method on ImageNet and Hànzì dataset, which is not stable. Based on Eq. (5), *Noise2Same* should achieve the best performance when the standard deviation of noise σ_n is known. However, *Noise2Info* (without knowing σ_n) even outperforms *Noise2Same* ($\sigma_{loss} = \sigma_n$) on ImageNet and Hànzì. That is because the noises of these two data sets are not zero-mean, which do not follow the assumption of $\mathcal{J}$-invariant models. We can also observe that *Noise2Same* ($\sigma_{loss} = \sigma_n$) is slightly better than *Noise2Info* on the zero-mean data BSD68. Overall, *Noise2Info* achieves good performance

Table 4: The performance on the Hànzì dataset injected with Gaussian noise of standard deviation $\sigma'_n \in [0.3, 0.5, 0.7, 0.9]$. Our *Noise2Info* is compared with *Noise2Same*, which set $\sigma_{loss} = 1$, $\sigma_{loss} = \sigma'_n$ and the correct ideal case $\sigma_{loss} = \sigma_n = \sigma'_n / \sqrt{(\sigma'_n)^2 + \sigma^2_{Y'}}$. The best scores are in **bold** font and the second-best scores are underlined.

Model	Level of injected Gaussian noise							
	$\sigma'_n = 0.3$		$\sigma'_n = 0.5$		$\sigma'_n = 0.7$		$\sigma'_n = 0.9$	
	PSNR	σ_{loss}	PSNR	σ_{loss}	PSNR	σ_{loss}	PSNR	σ_{loss}
Noise2Void	23.60	-	20.48	-	18.04	-	16.25	
Noise2Self	23.45	-	20.56	-	18.22	-	16.58	-
Noise2Same ($\sigma_{loss} = \sigma'_n$)	11.70	0.3	10.85	0.5	11.73	0.7	16.64	0.9
Noise2Same ($\sigma_{loss} = \sigma_n$)	**23.81**	0.5845	20.56	0.7683	18.62	0.8593	16.71	0.9075
Noise2Same ($\sigma_{loss} = 1$)	23.55	1.0	20.78	1.0	18.66	1.0	**16.82**	1.0
Noise2Info	23.73	0.6006	**20.81**	0.7818	**18.67**	0.8710	16.80	0.9187

among self-supervised modes without requiring information about clean images, noise, and noise model.

4.3. The estimation of σ_n in Noise2Info

The key component of *Noise2Info* is to estimate σ_n as the σ_{loss} in training (see Sec. 3.1 and Algo. 1). As shown in Tab. 3, we list the final derived σ_{loss} of *Noise2Info* on three benchmark data sets. We can observe that the derived σ_{loss} is very close to the true σ_n. In BSD68, the derived σ_{loss} is slightly higher than σ_n, which follows the theory in Eq. (6). However, the derived σ_{loss} is even lower than σ_n on other data sets because the assumption of zero-mean does not strictly hold. Specifically, the performances of *Noise2Info* (PSNR = 22.51, 22.60) is pretty close to *Noise2Same* (PSNR = 22.49, 22.63) on ImageNet. The reason might be that σ_{loss} and σ_n are pretty close to 1. For Hànzì, hard clipping is applied and the σ_n is even larger than 1. The results of *Noise2Info* (PSNR = 14.43, 14.43) are slightly higher than those of self-supervised *Noise2Same*(PSNR = 14.38, 14.36) and much higher than those of *Noise2Same* with $\sigma_{loss} = \sigma_n$ (PSNR = 14.14, 14.08). As BSD68 follows zero-mean Gaussian noise, Noise2Info extracts σ_{loss} (0.5357, 0.5309) when $\sigma_n = 0.5043$.

Besides, Proposition 1 states that *Noise2Info*'s estimation will be closer to σ_n as training steps increase. Besides, we plot Fig. 4 to show the change of σ_{loss} derivation during training. Note that we add Gaussian noise with zero mean into clean images in Hànzì data since it does not follow the assumption of $\mathcal{J}$-invariant models. We can observe that Fig. 4 indeed validates the claims in Proposition 1.

4.4. The influence of σ_n

To further study the influence of σ_n to *Noise2Same* with $\sigma_{loss} = 1$ and *Noise2Info*, we construct noisy images based on the clean images of Hànzì [3], where the added noises are Gaussian noise with different σ_n. To construct a dataset, each original clean image Y' is applied with a noise map N' with std σ'_n to get noisy image X'. After normalizing X' to

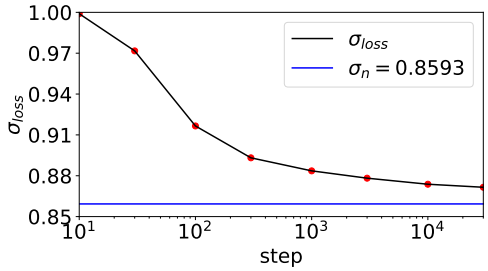

(a) Hànzì data set.

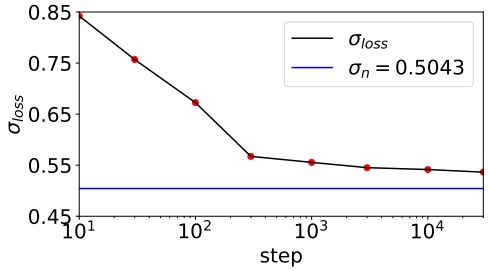

(b) BSD68 data set.

Figure 4: σ_{loss} estimation in different training steps.

X, σ'_n is usually different from σ_n. Assume that the standard deviation of original clean and noisy images are $\sigma_{Y'}$ and $\sigma_{X'}$, we have: $\sigma_n = \sigma'_n / \sigma_{X'} = \sigma'_n / \sqrt{(\sigma'_n)^2 + \sigma^2_{Y'}}$, where $\sigma^2_{X'} = (\sigma'_n)^2 + \sigma^2_{Y'}$ as noise is independent to the clean images. The model replaces masking values with random samples, and other implementations are the same as Sec. 4.1. As shown in Tab. 4, *Noise2Info* successfully estimates σ_{loss} which closely upper bounds the real σ_n. When σ_n is small, *Noise2Info* stably performs better than *Noise2Same* with $\sigma_{loss} = 1$ and close to the ideal result from *Noise2Same* with $\sigma_{loss} = \sigma_n$. With σ_n close to 1, the σ_{loss} and PSNR of the 3 methods are close to each other. Except for Gaussian distribution, we further study the influence of more noise distributions in Appx. F.2.

Table 5: The performance on the Hànzì dataset on more noise types. N2S denotes Noise2Same ($\sigma_{loss} = \sigma_n$). FBI [6] is a denoising method designed for Poisson-Gaussian noise.

Model	Types of injected noises					
	Poisson-Gaussian (A) $\sigma_n = 0.8181, \mu = 0.0002$		Poisson-Gaussian (B) $\sigma_n = 10.32, \mu = 6.34$		Pepper $\sigma_n = 0.8492, \mu = 0.3037$	
	PSNR	σ_{loss}	PSNR	σ_{loss}	PSNR	σ_{loss}
Noise2Void	18.88	-	17.93	-	23.77	-
Noise2Self	18.91	-	17.57	-	22.19	-
Noise2Same	18.91	0.8181	14.49	10.32	24.35	0.8492
FBI [6]	18.87	N/A	6.54	N/A	N/A	N/A
Noise2Info	**19.11**	0.8317	**18.52**	0.8551	**24.96**	0.7043

4.5. Further Analysis on Limitation of Noise2Info

The theory of Noise2Info mainly follows the assumption of $\mathcal{J}$-invariant models where the noise in images is zero-mean and signal independent. Here we further analyze the limitations of *Noise2Info* caused by such an assumption.

As we discussed in Tab. 3, the upper bound estimation in *Noise2Info* is not quite accurate in the non-zero mean case. Thus, we use Fig. 3 and Tab. 4 to show that the theory of *Noise2Info* indeed holds for the zero-mean case. Besides, the empirical performance of *Noise2Info* is still stable for datasets without the zero-mean assumption. For example, in Tab. 2, *Noise2Info* is better than other self-supervision methods, though the noise is not zero-mean for Hànzì and not zero-mean nor signal-independent for ImageNet. This validates the generality of *Noise2Info*.

The signal independent assumption is adopted by many denoising methods [29, 3, 17, 8, 18, 9]. Other than that, some works focus on particular noises such as Poisson-Gaussian noise and Pepper noise to mimic real world scenarios [6, 7]. Therefore, we conduct more experiments on these noises together with non-zero mean assumption in Tab. 5. Poisson-Gaussian noise and pepper noise are both non-zero-mean without fixed variance. For Poisson-Gaussian noise on clean image Y, a standard setting is of the form: $X = aP(Y) + N(b)$, where $P(Y)$ is sampled from a Poisson distribution with variance Y and N is sampled from Gaussian distribution $\mathcal{N}(0, b^2)$. We use 2 groups of parameters $(a, b) = (1, 0.3)$ and $(0.05, 0.02)$, denoted as Poisson-Gaussian A and B, where A is set to be zero-mean. Pepper noise randomly sets a pixel to 0 with $p = 0.25$. As shown in Tab. 5 with the state-of-art work for Poisson-Gaussian noise (FBI [6]), *Noise2Info* still performs best.

Besides, we conduct experiments on real world datasets, which is discussed in Appx. E. Though inferior to Noise2Same due to special distribution given in Table. 7, our method outperforms other self-supervised methods.

5. Conclusion

In this paper, we propose *Noise2Info* for self-supervised image denoising, which extracts information of noise only based on noisy images. Compared with methods that require clean images or noisy image pairs, self-supervised models are mostly developed based on the theory of $\mathcal{J}$-invariance. It could be further improved if σ_n of noise is known. However, it is intractable without the clean images and distribution of noise. In *Noise2Info*, we first present a theoretical upper bound for σ_n, and propose a tractable estimation σ_n only based on noisy images. Then, we prove that the estimation is more accurate when the model is more powerful and propose a training framework that takes turns to estimate σ_n and update the model. Extensive experiments are conducted on benchmark datasets and synthetic datasets with different scales of noise and different types of noise. The results show that *Noise2Info* effectively denoises images and tightly bounds the σ_n.

Acknowledgement

Lei Chen's work is partially supported by National Key Research and Development Program of China Grant No. 2022YFE0200500 and 2018AAA0101100, the Hong Kong RGC GRF Project 16213620, CRF Project C6030-18G, C1031-18G, C5026-18G, CRF C2004-21GF, AOE Project AoE/E603/18, RIF Project R6020-19, Theme-based project TRS T41-603/20R, China NSFC No. 61729201, Guangdong Basic and Applied Basic Research Foundation 2019B151530001, Hong Kong ITC ITF grants ITS/044/18FX and ITS/470/18FX, Microsoft Research Asia Collaborative Research Grant, HKUST-NAVER/LINE AI Lab, Didi-HKUST joint research lab, HKUST-Webank joint research lab grants and HKUST Global Strategic Partnership Fund (2021 SJTU-HKUST). Shimin Di's work is supported by the JC STEM Lab of Data Science Foundations funded by The Hong Kong Jockey Club Charities Trust. Shimin Di is the Corresponding Author.

References

[1] Martín Abadi, Paul Barham, Jianmin Chen, Zhifeng Chen, Andy Davis, Jeffrey Dean, Matthieu Devin, Sanjay Ghemawat, Geoffrey Irving, Michael Isard, Manjunath Kudlur, Josh Levenberg, Rajat Monga, Sherry Moore, Derek Gordon Murray, Benoit Steiner, Paul A. Tucker, Vijay Vasudevan, Pete Warden, Martin Wicke, Yuan Yu, and Xiaoqiang Zheng. Tensorflow: A system for large-scale machine learning. In OSDI, 2016. 6

[2] Abdelrahman Abdelhamed, Stephen Lin, and Michael S. Brown. A high-quality denoising dataset for smartphone cameras. In CVPR, 2018. 6, 12

[3] Joshua Batson and Loïc Royer. Noise2self: Blind denoising by self-supervision. In ICML, 2019. 1, 3, 4, 6, 7, 8, 9, 14

[4] Antoni Buades, Bartomeu Coll, and Jean-Michel Morel. A non-local algorithm for image denoising. In CVPR (2), 2005. 3, 6, 7

[5] Antoni Buades, Bartomeu Coll, and Jean-Michel Morel. A review of image denoising algorithms, with a new one. Multiscale modeling & simulation, (2), 2005. 1, 3

[6] Jaeseok Byun, Sungmin Cha, and Taesup Moon. Fbi-denoiser: Fast blind image denoiser for poisson-gaussian noise. In CVPR, 2021. 9

[7] Jaeseok Byun and Taesup Moon. Learning blind pixelwise affine image denoiser with single noisy images. IEEE Signal Process. Lett., 2020. 9

[8] Sungmin Cha, Taeeon Park, Byeongjoon Kim, Jongduk Baek, and Taesup Moon. GAN2GAN: generative noise learning for blind denoising with single noisy images. In ICLR, 2021. 6, 9

[9] Jingwen Chen, Jiawei Chen, Hongyang Chao, and Ming Yang. Image blind denoising with generative adversarial network based noise modeling. In CVPR, 2018. 9

[10] Kostadin Dabov, Alessandro Foi, Vladimir Katkovnik, and Karen O. Egiazarian. Image denoising by sparse 3-d transform-domain collaborative filtering. IEEE Trans. Image Process., (8), 2007. 1, 3, 6, 7

[11] Weisheng Dong, Lei Zhang, Guangming Shi, and Xin Li. Nonlocally centralized sparse representation for image restoration. IEEE Trans. Image Process., (4), 2013. 1

[12] Shuhang Gu, Lei Zhang, Wangmeng Zuo, and Xiangchu Feng. Weighted nuclear norm minimization with application to image denoising. In CVPR, 2014. 1

[13] Frederic Guichard, Jean-Michel Morel, and R Ryan. Image analysis and pdes. preprint, 2001. 3

[14] Shi Guo, Zifei Yan, Kai Zhang, Wangmeng Zuo, and Lei Zhang. Toward convolutional blind denoising of real photographs. In CVPR, 2019. 1, 3

[15] Godfrey Harold Hardy, John Edensor Littlewood, George Pólya, György Pólya, et al. Inequalities. Cambridge university press, 1952. 11

[16] Kaiming He, Xiangyu Zhang, Shaoqing Ren, and Jian Sun. Deep residual learning for image recognition. In CVPR, 2016. 1

[17] Alexander Krull, Tim-Oliver Buchholz, and Florian Jug. Noise2void - learning denoising from single noisy images. In CVPR, 2019. 1, 3, 4, 6, 7, 9

[18] Samuli Laine, Tero Karras, Jaakko Lehtinen, and Timo Aila. High-quality self-supervised deep image denoising. In NeurIPS, 2019. 1, 3, 4, 6, 7, 9

[19] Jaakko Lehtinen, Jacob Munkberg, Jon Hasselgren, Samuli Laine, Tero Karras, Miika Aittala, and Timo Aila. Noise2noise: Learning image restoration without clean data. In ICML, 2018. 1, 3, 6, 7

[20] David R. Martin, Charless C. Fowlkes, Doron Tal, and Jitendra Malik. A database of human segmented natural images and its application to evaluating segmentation algorithms and measuring ecological statistics. In ICCV, 2001. 6

[21] Nick Moran, Dan Schmidt, Yu Zhong, and Patrick Coady. Noisier2noise: Learning to denoise from unpaired noisy data. In CVPR, 2020. 1

[22] Haoyu Ren, Mostafa El-Khamy, and Jungwon Lee. Dn-resnet: Efficient deep residual network for image denoising. In ACCV (5), 2018. 1

[23] Olaf Ronneberger, Philipp Fischer, and Thomas Brox. U-net: Convolutional networks for biomedical image segmentation. In MICCAI (3), 2015. 1

[24] Richard J Rossi. Mathematical statistics: an introduction to likelihood based inference. John Wiley & Sons, 2018. 5

[25] Olga Russakovsky, Jia Deng, Hao Su, Jonathan Krause, Sanjeev Satheesh, Sean Ma, Zhiheng Huang, Andrej Karpathy, Aditya Khosla, Michael S. Bernstein, Alexander C. Berg, and Li Fei-Fei. Imagenet large scale visual recognition challenge. Int. J. Comput. Vis., (3), 2015. 6

[26] Chunwei Tian, Lunke Fei, Wenxian Zheng, Yong Xu, Wangmeng Zuo, and Chia-Wen Lin. Deep learning on image denoising: An overview. Neural Networks, 2020. 1, 3

[27] Zhengyang Wang, Yaochen Xie, and Shuiwang Ji. Global voxel transformer networks for augmented microscopy. Nat. Mach. Intell., (2), 2021. 7

[28] Martin Weigert, Uwe Schmidt, Tobias Boothe, Andreas Müller, Alexandr Dibrov, Akanksha Jain, Benjamin Wilhelm, Deborah Schmidt, Coleman Broaddus, Siân Culley, et al. Content-aware image restoration: pushing the limits of fluorescence microscopy. Nature methods, (12), 2018. 13

[29] Yaochen Xie, Zhengyang Wang, and Shuiwang Ji. Noise2same: Optimizing A self-supervised bound for image denoising. In NeurIPS, 2020. 1, 2, 3, 4, 6, 7, 9, 11, 13

[30] Jun Xu, Hui Li, Zhetong Liang, David Zhang, and Lei Zhang. Real-world noisy image denoising: A new benchmark. CoRR, 2018. 6, 12

[31] Kai Zhang, Wangmeng Zuo, Yunjin Chen, Deyu Meng, and Lei Zhang. Beyond a gaussian denoiser: Residual learning of deep CNN for image denoising. IEEE Trans. Image Process., (7), 2017. 1, 3

A. Proof of Lemma 1

Proof. Recall that *Noise2Same* [29] introduces the following inequation:

$$\mathbb{E}_{X,Y}\left[||\mathcal{F}(X)-Y||^2+||X-Y||^2\right]\leq\mathcal{L}_{in}+2\sigma_n\cdot\mathcal{L}_{ex}.$$

Based on the assumption of zero-mean noise, the left-hand side satisfies:

$$\begin{aligned}&\mathbb{E}_{X,Y}\left[||\mathcal{F}(X)-Y||^2+||X-Y||^2\right]\\=&\mathbb{E}_{X,Y}\left[||\mathcal{F}(X)-Y||^2+||X-Y||^2\right]-\left(\mathbb{E}_{X,Y}\left[X-Y\right]\right)^2\\=&\mathbb{E}_{X,Y}\left[||\mathcal{F}(X)-Y||^2\right]+Var\left(X-Y\right)\\=&\mathbb{E}_{X,Y}\left[||\mathcal{F}(X)-Y||^2\right]+m\sigma_n^2.\end{aligned}\tag{11}$$

Eq. (11) holds as m pixels in each noise map $(X-Y)$ are independent and identically distributed. Reorganizing the inequation, we have:

$$\sigma_n\leq\frac{\mathcal{L}_{ex}+\sqrt{\mathcal{L}_{ex}^2+m(\mathcal{L}_{in}-\mathbb{E}_{X,Y}\left[||\mathcal{F}(X)-Y||^2\right])}}{m},$$

□

B. Proof of Lemma 2

Proof. As we do not restrict the distribution of n^*, we have the likelihood estimation function:

$$L(\mathbf{P}_{\tilde{\mathbf{n}}}|\tilde{\mathbf{n}})=\prod_{\tilde{N}_j^{(i)}\in\tilde{\mathbf{n}}}P_{\tilde{N}_j^{(i)}},$$

where $\tilde{\mathbf{n}}$ is the set of mq pixels of removed noise from q images of size m. $\mathbf{P}_{\tilde{\mathbf{n}}}$ are the set of probabilities corresponding to $\tilde{\mathbf{n}}$ of distribution n^*, which has no specified correlation with each other. Taking the *log*, we want to maximize:

$$\log L(\mathbf{P}_{\tilde{\mathbf{n}}}|\tilde{\mathbf{n}})=\sum_{\tilde{N}_j^{(i)}\in\tilde{\mathbf{n}}}\log P_{\tilde{N}_j^{(i)}}$$

As the sum of all the probabilities in a distribution equals to 1, we have:

$$\sum_{\tilde{N}_j^{(i)}\in\tilde{\mathbf{n}}}P_{\tilde{N}_j^{(i)}}\leq 1$$

The constrained optimization problem can be solved using Lagrange multipliers. We construct:

$$\mathcal{L}(\mathbf{P}_{\tilde{\mathbf{n}}};\lambda)=\sum_{\tilde{N}_j^{(i)}\in\tilde{\mathbf{n}}}\log P_{\tilde{N}_j^{(i)}}+\lambda\sum_{\tilde{n}\in\tilde{\mathbf{n}}}P_{\tilde{N}_j^{(i)}}\leq 1$$

By solving:

$$\begin{cases}\dfrac{\partial\mathcal{L}(\mathbf{P}_{\tilde{\mathbf{n}}};\lambda)}{\partial P_{\tilde{N}_j^{(i)}}}=0 & \forall P_{\tilde{N}_j^{(i)}}\in\mathbf{P}_{\tilde{\mathbf{n}}}\\ \dfrac{\partial\mathcal{L}(\mathbf{P}_{\tilde{\mathbf{n}}};\lambda)}{\partial\lambda}=0\end{cases},$$

we have:

$$P_{\tilde{N}_j^{(i)}}=\frac{1}{|\mathbf{P}_{\tilde{\mathbf{n}}}|}=\frac{1}{mq}\qquad\forall P_{\tilde{N}_j^{(i)}}\in\mathbf{P}_{\tilde{\mathbf{n}}}$$

As $\sum_{P_{\tilde{N}_j^{(i)}}\in\mathbf{P}_{\tilde{\mathbf{n}}}}=1$, we have the close-form probability distribution of the maximum likelihood estimation as:

$$P(n^*=\tilde{N}_j^{(i)})=P_{\tilde{N}_j^{(i)}}=\frac{1}{mq}\qquad\forall\tilde{N}_j^{(i)}\in\tilde{\mathbf{n}}$$

□

C. Proof of Lemma 3

Proof.

$$\begin{aligned}&\mathbb{E}_{N^*}\left[\mathbb{E}_X\left[\sum_{j=1}^m(N_j^*-\tilde{N}(X)_j)^2\right]\right]\\=&\mathbb{E}_{N^*}\left[\mathbb{E}_X\left[\sum_{j=1}^m((N_j^*)^2+\tilde{N}(X)_j^2)-2\sum_{j=1}^m(N_j^*\cdot\tilde{N}(X)_j)\right]\right]\\=&\mathbb{E}_{N^*}\left[\mathbb{E}_X\left[\sum_{j=1}^m((N_{v_j}^*)^2+\tilde{N}(X)_{u_j}^2)-2\sum_{j=1}^m(N_j^*\cdot\tilde{N}(X)_j)\right]\right]\\\geq&\mathbb{E}_{N^*}\left[\mathbb{E}_X\left[\sum_{j=1}^m((N_{v_j}^*)^2+\tilde{N}(X)_{u_j}^2)-2\sum_{j=1}^m(N_{v_j}^*\cdot\tilde{N}(X)_{u_j})\right]\right]\\=&\mathbb{E}_{N^*}\left[\mathbb{E}_X\left[\sum_{j=1}^m(N_{v_j}^*-\tilde{N}(X)_{u_j})^2\right]\right].\end{aligned}\tag{12}$$

Eq. 12 applied the rearrangement inequality [15]. □

D. Proof of Proposition 1

Proof. The relaxations that go tighter when $\mathcal{F}(X)$ is close to Y are enumerated and proved here:

- Our estimation is based on the right hand side of Ineq. (6):

  $$\sigma_n\leq\frac{\mathcal{L}_{ex}+\sqrt{\mathcal{L}_{ex}^2+m(\mathcal{L}_{in}-\mathbb{E}_{X,Y}\left[||\mathcal{F}(X)-Y||^2\right])}}{m}$$

  During training, we minimize loss $\mathcal{L}(\mathcal{F},X)=\mathcal{L}_{in}+2\sigma_{loss}\mathcal{L}_{ex}$, so that the terms $\mathcal{L}_{ex}$ and $\mathcal{L}_{in}$ are getting smaller and makes the bound tighter. The remaining thing is to show that the estimation through Eq. (7-10) for the lower bound of $\mathbb{E}_{X,Y}\left[||\mathcal{F}(X)-Y||^2\right]$ is getting tighter as well.

- In Eq. (9), MLE $\mathscr{N}^*$ replaces the true noise distribution $\mathscr{N}$ as an estimation. When $\mathcal{F}(X)$ is closer to Y,

the removed noise $X-\mathcal{F}(X)$ is closer to $N=X-Y$. As N is sampled from $\mathcal{N}$, $\mathcal{N}^*$ based on $X-\mathcal{F}(X)$ is closer to the distribution of $\mathcal{N}^*$.

- In Ineq. (12), the conditions for its equality is that larger removed noise maps to larger real noise. In other words, the j^{th} largest pixel of $X-\mathcal{F}(X)$ has the same index as the j^{th} largest pixel of $X-Y$, which tends to hold more strictly when $\mathcal{F}(X)$ is closer to Y. Formally, assuming that the pixels with index i and j in removed noise $X-F(X)$ (denoted as rf_i and rf_j) and those in real noise $X-Y$ (denoted as ry_i and ry_j) are disordered (i.e., $(rf_i-rf_j)(ry_i-ry_j)<0$), then by exchanging them ($rf_i^*=rf_j, rf_j^*=rf_i$) to get an output $F^*(X)$ with ordered pair, we have $||Y-F^*(X)||^2 < ||Y-F(X)||^2$. To prove it, we show $||Y-F^*(X)||^2-||Y-F(X)||^2<0$ as follows:

$$
\begin{aligned}
&||Y-F^*(X)||^2-||Y-F(X)||^2\\
=&||(X-F^*(X))-(X-Y)||^2-||(X-F(X))-(X-Y)||^2\\
=&\sum_k(rf_k^*-ry_k)^2-\sum_k(rf_k-ry_k)^2\\
=&\sum_{k\neq i,j}((rf_k^*-ry_k)^2-(rf_k-ry_k)^2)\\
&+(rf_i^*-ry_i)^2+(rf_j^*-ry_j)^2-(rf_i-ry_i)^2-(rf_j-ry_j)^2\\
=&(rf_i^*-ry_i)^2+(rf_j^*-ry_j)^2-(rf_i-ry_i)^2-(rf_j-ry_j)^2\\
=&(rf_j-ry_i)^2+(rf_i-ry_j)^2-(rf_i-ry_i)^2-(rf_j-ry_j)^2\\
=&(rf_j-ry_i)^2-(rf_i-ry_i)^2+(rf_i-ry_j)^2-(rf_j-ry_j)^2\\
=&(rf_j-rf_i)(rf_j+rf_i-2ry_i)+(rf_i-rf_j)(rf_i+rf_j-2ry_j)\\
=&(rf_j-rf_i)(rf_j+rf_i-2ry_i-rf_i-rf_j+2ry_j)\\
=&(rf_j-rf_i)(-2ry_i+2ry_j)\\
<&0
\end{aligned}
$$

□

Table 6: The performance on the real world datasets SIDD and PolyU. We compare our *Noise2Info* with Noisy image without clean, supervised method *Noise2True*, self-supervised method with noise information *Noise2Same* ($\sigma_{loss}=\sigma_n$), and pure self-supervised methods *Noise2Void*, *Noise2Self*, *Noise2Same* ($\sigma_{loss}=1$). The best score is in **bold** font and the second-best scores are underlined.

Model	**Data set**	
	SIDD	PolyU
Noisy image	15.45	35.62
Noise2True	23.82	36.43
Noise2Same ($\sigma_{loss}=\sigma_n$)	16.26	36.09
ConvBS	13.73	30.32
Noise2Void	15.69	35.54
Noise2Self	15.94	34.23
Noise2Same ($\sigma_{loss}=1$)	**19.99**	**36.72**
Noise2Info	<u>16.07</u>	<u>35.76</u>

Table 7: The information of groundtruth σ_n and σ_{loss} derived by *Noise2Info* on SIDD and PolyU data sets.

Data set	Training Set		Test Set		*N2I*
	μ_n	σ_n	μ_n	σ_n	σ_{loss}
SIDD	-0.006	0.057	-0.011	0.074	0.022
PolyU	0	0.097	-0.005	0.177	0.026

Table 8: The statistics of dataset Planaria. We show the standard deviation and min-max values of 1) noisy images X from the training dataset; 2) noisy images X from three groups of testing dataset; and 3) clean images Y from the testing dataset.

	Train	Test			
	X	X (C1)	X (C2)	X (C3)	Y
σ	0.1858	59.62	46.22	36.58	1532
min value	-0.5888	253	293	295	265
max value	87.94	36824	1632	1277	51061

E. Analysis on Real-world Datasets

E.1. SIDD Dataset & PolyU Dataset

In this subsection, we display experimental results on two real-world datasets SIDD [2] and PolyU [30].

SIDD dataset [2] includes images captured by five smartphone cameras in 10 static scenes. The training dataset contains 320 image pairs where 1280 image pairs are for testing. The results are given in Table. 6. Note that we normalize both input and output so that the PSNR score is relatively smaller compared with published scores [2].

PolyU dataset [30] contains 40 large raw images and crops 100 regions of 512×512 from them. The authors capture each scene many times and treat the mean of these images as the "ground truth" image. We use the first 50 cropped regions for training and the latter 50 for testing. The results are shown in Table. 6.

It is surprising that our method is slightly inferior to the ideal case of Noise2Same models ($\sigma_{loss}=\sigma_n$) but largely falls behind Noise2Same with $\sigma_n=1$. We collect the statistics of SIDD dataset and PolyU dataset in Table. 7 and found that their standard deviations of testing datasets are inconsistant with those of training datasets. Besides, SIDD has noise of $\mu=-0.011$ while $\sigma_n=0.074$, where its mean is not neglectable compared with its std. We argue that these facts breaks the assumptions of listed self-denoising methods inluding Noise2Info, where larger σ_{loss} leads to a better result. It is interesting that on SIDD, self-supervised methods have large gaps compared to supervised method (PSNR$\leq$19.99 against 23.82), while on PolyU, Noise2Same even outperforms the supervised method (PSNR=36.72 against 36.43), which implies possible merits for future works. In addition, SIDD and PolyU have smaller σ_n on their training set (0.057 and 0.097) than

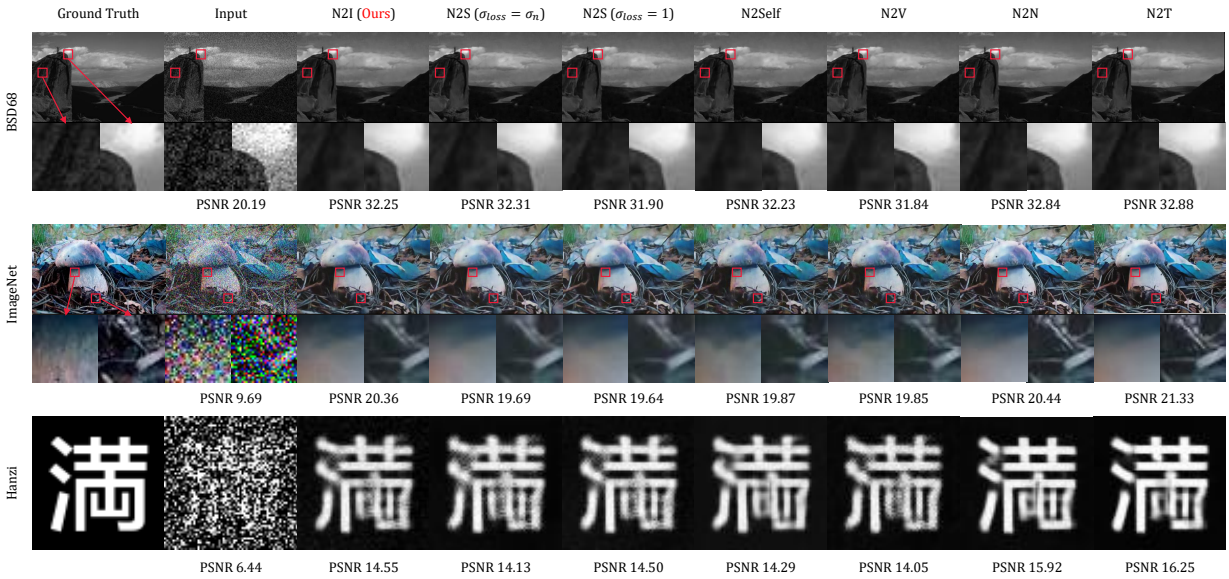

Figure 5: Result demonstration without cherry-picking. We display outputs of methods including *N2I*, two versions of *Noise2Same*, *Noise2Self*, *Noise2Void*, *Noise2Noise*, and *Noise2True* with their PSNRs of 3 figures from 3 datasets.

Table 9: The performance on the Hànzì dataset with different types of noise. We compare our *Noise2Info* with *Noise2Same* trained under $\sigma_{loss} = 1$ and the intractable ideal case $\sigma_{loss} = \sigma_n$. All the noises are of std 0.3, including Gaussian noise, Logistic Noise, Uniform noise, and the mixture of these 3 noises. The best scores are in **bold** font and the second-best scores are underlined.

Model	**Types of injected noises** (σ_n =0.5845)							
	Gaussian noise		Logistic noise		Uniform noise		Mixed noise	
	PSNR	σ_{loss}	PSNR	σ_{loss}	PSNR	σ_{loss}	PSNR	σ_{loss}
Noise2Void	23.60	-	23.15	-	23.32	-	23.13	-
Noise2Self	23.45	-	**23.67**	-	11.79	-	23.45	-
Noise2Same ($\sigma_{loss} = \sigma_n$)	**23.81**	0.5845	23.17	0.5845	**24.20**	0.5845	23.44	0.5845
Noise2Same ($\sigma_{loss} = 1$)	23.55	1.0	23.42	1.0	23.64	1.0	<u>23.50</u>	1.0
Noise2Info	<u>23.73</u>	0.6006	<u>23.44</u>	0.5986	<u>23.88</u>	0.6006	**23.76**	0.6008

those on their testing set (0.074 and 0.177), which leads to a smaller estimation of $N2I$ and a weaker result compared to Noise2Same. However, Noise2Info still outperforms other self-supervised methods.

E.2. Planaria Dataset

Planaria [28] is a dataset with physically acquired 3D fluorescence microscopy data. For training, 17005 3D patches of noisy images at three noise levels are collected under conditions C1, C2, and C3. Twenty images at each of the three noise levels are used for testing. However, when we investigate the statistics of the Planaria dataset, we found that its σ_n is not consistent in training and testing datasets with pretty different scales.

In Tab. 8, we collect the standard deviation and min-max values of each groups of clean and noisy images. The scale of them varies a lot. We follow the previous setting [29] to normalize each group including the clean image for training and evaluation, where on the other datasets, output $\mathcal{F}(X)$ is denormalized and compared with the original Y. In this setting, we found that the standard deviations σ_n of noises under the three conditions are $0.98, 1.13, 1.32$, where the extracted σ_{loss} on training dataset using *Noise2Info* is 0.1612. *Noise2Same* [29] uses $\sigma_{loss} = 1$, which fits to the testing datasets. However, as the assumptions that σ_n should be consistent in training and testing datasets is not held, *Noise2Info* is not a suitable choice for Planaria.

F. More Experimental Results

F.1. Visual Cases on Three Datasets

Fig. 5 shows the output samples of the compared methods. *Noise2Same* with known σ_n and our *Noise2Info* outperform other self-supervised methods and are comparable

with the two supervised methods. With supervision, supervised methods are capable to learn structured features such as the strokes of Hànzì, which is a weak point for self-supervised methods as well-defined smooth strokes are never seen. In contrast, the gap between our method and supervised methods are smaller for the other two real world datasets.

F.2. Insight: Different Noise Models

We further investigate the influence of different noise models with zero-mean. Gaussian noise, logistic noise, uniform noise, and the mixture of the three are added to the clean Hànzì [3]. All the images have added noise of std $\sigma_n' = 0.3$.

We show the results in Tab. 9. For all the noises, *Noise2Info* bounds σ_n tightly and gets stable results. Datasets with Gaussian and Uniform noise follow our theory, where *Noise2Same* with ideal σ_{loss} performs best and *Noise2Info* is the second-best. For the Logistic and Mixed noises, our *Noise2Info* even performs better than *Noise2Same*. *Noise2Self* performs unstably with the best score for Logistic noise but collapes on Uniform noise.